

Journal of
Mechanics of
Materials and Structures

**STATIC ANALYSIS OF MASONRY VAULTS, CONSTITUTIVE
MODEL
AND NUMERICAL ANALYSIS**

Massimiliano Lucchesi, Cristina Padovani, Giuseppe Pasquinelli
and Nicola Zani

Volume 2, N° 2

February 2007

STATIC ANALYSIS OF MASONRY VAULTS, CONSTITUTIVE MODEL AND NUMERICAL ANALYSIS

MASSIMILIANO LUCCHESI, CRISTINA PADOVANI, GIUSEPPE PASQUINELLI AND NICOLA ZANI

The paper deals with some of the explicit and numerical methods used for modeling the mechanical behavior of masonry vaults and domes. After a brief description of the constitutive equation of masonry-like materials, a numerical method for the structural analysis of masonry vaults is presented. Then, the concept of maximum modulus eccentricity surface for masonry vaults is recalled. Subsequently, the collapse load and the corresponding mechanism are explicitly calculated for two particular cases: a circular plate subjected to a permanent load acting on the lateral surface and a variable vertical load applied to the extrados, and a spherical dome subjected to its own weight and variable point load applied to the keystone. The exact solutions are compared to the numerical results obtained via finite element analysis. Lastly, a study of the dome of the church of Santa Maria Maddalena in Morano Calabro is described. The method has enabled the stress field and the fractures distribution in the dome to be determined and the maximum modulus eccentricity surface to be evaluated.

1. Introduction

Many historically and artistically important masonry buildings of the world's architectural heritage are in dire need of maintenance and restoration. In order to optimize such operations in terms of cost-effectiveness, architectural impact and static effectiveness, accurate models of the structural behavior of masonry constructions are invaluable. The ultimate aim of such modeling is to obtain important information, such as the stress field, and to estimate the extent of cracking and its evolution when the structure is subjected to variations in loading conditions.

Although masonry has been used in building for centuries, it is only recently that constitutive models and calculation techniques have been available that enable realistic description of the static behavior of structures made of this heterogeneous material, whose response to tension is fundamentally different from the response to compression. Thus, with the aim of determining the collapse load for masonry structures, many authors have proposed rigid blocks models with different kind of interfaces [Livesley 1978; 1992b], and apply these models to the study of vaults as well [Orduña and Lourenço 2003]. The elastic-plastic model is widely adopted; see, for example, [Lourenço and Rots 1997; Lourenço et al. 1998]. A comparison among different models of this type can be found in [Genna et al. 1998], and an application to the study of vaults is presented in [Theodossopoulos et al. 2002]. Many models have been proposed that, by using homogenization techniques, allow one to take into account the masonry texture, their application is in general limited to the study of panels [Luciano and Sacco 1997; Maier et al. 1992; Trovalusci and Masiani 2005].

Keywords: masonry vaults, nonlinear elasticity, finite-element method, static analysis, limit analysis.

A constitutive equation widely adopted to model the behavior of masonry materials considers them as nonlinear elastic materials with zero tensile strength and infinite compressive strength [Signorini 1925a; 1925b; Heyman 1966; 1982; Di Pasquale 1992; Del Piero 1989; Panzeca and Polizzotto 1988; Como 1992]. This equation, known as the *masonry-like* or *no-tension* model, can, at least in certain aspects, realistically describe the mechanical behavior of masonry [Bernardeschi et al. 2004; Lucchesi et al. 1996].

Despite the relative simplicity of the constitutive equation of masonry-like materials, explicit solution of equilibrium problems of any practical interest is nonetheless very difficult [Bennati and Padovani 1997; Lucchesi and Zani 2003]. Therefore, in order to study real problems, it is necessary to resort to numerical methods. To this end, suitable numerical techniques have been developed [Lucchesi et al. 1994]. The constitutive models and the numerical method studied have therefore been implemented into the finite element code NOSA [Lucchesi et al. 2000] developed at the Institute of Information Science and Technologies (ISTI) in Pisa. NOSA enables determination of the stress state and the presence of any cracking, as well as the modeling of any potential strengthening and restoration work, such as, for example, the fitting of rods and reinforcement rings.

The code has been successfully applied to the analysis of some buildings of historical and architectural interest, including S. Nicolò's Mother-House in Noto, the Goldoni Theatre in Livorno, the Medici Arsenal in Pisa, the Buti bell tower, and the Pisa church of San Pietro in Vinculis. These studies proved that even though the masonry-like model does not take into account, at least in its original formulation, some features such as material anisotropy, it allows one to conduct realistic analyses of complex structures with large dimensions as frequently encountered in the applications.

In this paper we propose a method for studying masonry vaults. The aim is to provide a computational tool that can be used both to evaluate the safety of masonry monuments, as well as to guide the choice of strengthening operations.

In Section 2, we describe the constitutive equation adopted to study the equilibrium problem of masonry vaults.

Section 3 deals with the numerical methods used for modeling the mechanical behavior of masonry vaults and domes implemented in the NOSA code. A shell element based on the Love-Kirchhoff shell theory [Nagtegaal and Slater 1981] employed for discretizing vaulted structures is described.

In Section 4, the concept of maximum modulus eccentricity surface (m.m.e.s.) is formulated with the aim of allowing concise, effective rendering of the results of finite-element analyses, as well as evaluation of the safety of vaults. In dealing with masonry vaults the m.m.e.s. plays a role analogous to that of line of thrust for arches. In addition, this surface can provide useful information about the possible collapse mechanism when the numerical analysis is performed by progressively increasing the load, until it is no longer possible to determine an admissible equilibrated solution. Then, it allows one to define for the vaults a geometric safety factor similar to that proposed for the arches by Heyman [1982; 1966]. The numerical method proposed in this paper with the consequent calculation of the m.m.e.s., allows one to analyze any kind of vault (masonry spire, fan vault, incomplete dome, et cetera), subjected to any type of static load — a problem that can be hard to solve by classical methods [Heyman 1977]. Moreover, for the different types of load, it is possible to determine the corresponding collapse multiplier. An interactive graphic code has moreover been developed for calculation and visualization of the m.m.e.s.

Section 5 provides some example applications. In particular, we explicitly solve the collapse problem for two distinct structures: a circular plate subjected to a permanent load acting on its lateral surface

and a variable vertical load acting on the extrados, and a spherical dome subjected to its own weight and a variable point load at the keystone. The explicit solutions are compared with the numerical results obtained with the NOSA code. Lastly, we describe a study of the dome of the Church of Santa Maria Maddalena in Morano Calabro. This study has been commissioned by the Office for the Arts and Environment of the Region of Calabria, which is conducting restoration interventions on the church. Finite element analysis has allowed determination of both the stress field and the distribution of fractures within the dome.

2. The constitutive equation

To model the mechanical behavior of the material, we use the constitutive equation of *masonry-like* or *no-tension* materials [Heyman 1982; Del Piero 1989; Lucchesi et al. 1994] which are assumed to be nonlinear hyperelastic, with zero tensile strength and infinite compressive strength.

The infinitesimal strain \mathbf{E} is the sum of an elastic part and a positive semidefinite fracture part: in symbols, $\mathbf{E} = \mathbf{E}^e + \mathbf{E}^f$. Moreover, the Cauchy stress \mathbf{T} , negative semidefinite and orthogonal to \mathbf{E}^f , depends linearly and isotropically on \mathbf{E}^e as

$$\mathbf{T} = 2\mu\mathbf{E}^e + \lambda \operatorname{tr}(\mathbf{E}^e)\mathbf{I},$$

with $\mu > 0$ and $\lambda \geq 0$ the Lamé moduli of the material. (We assume throughout that Poisson's ratio is nonnegative.)

Consider the vault element with thickness h shown in Figure 1. Let η_1 and η_2 be an orthogonal coordinate system, not necessarily the principal one, defined on the mean surface \mathfrak{S} , with $\zeta \in [-h/2, h/2]$ as the coordinate in the normal direction \mathbf{n} . Denote by \mathbf{g}_1 and \mathbf{g}_2 the unit tangent vectors to η_1 and η_2 axis, respectively.

We assume that for each $\mathbf{p} \in \mathfrak{S}$ and $\zeta \in [-h/2, h/2]$, the stress tensor \mathbf{T} satisfies the condition

$$\mathbf{T}(\mathbf{p}, \zeta)\mathbf{n}(\mathbf{p}) = \mathbf{0}, \quad (1)$$

\mathbf{T} can be expressed as a nonlinear function of the total strain \mathbf{E} , $\mathbf{T} = \widehat{\mathbf{T}}(\mathbf{E})$, by using the coaxiality of \mathbf{E} , \mathbf{T} and \mathbf{E}^f , and taking into account assumption (1); see [Lucchesi et al. 1994]. To this purpose, we indicate with the same symbols the restrictions of \mathbf{E} , \mathbf{T} and \mathbf{E}^f to the two-dimensional linear space generated by \mathbf{g}_1 and \mathbf{g}_2 .

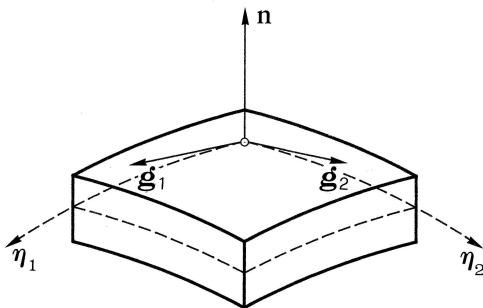


Figure 1. Vault element.

Let $e_1 \leq e_2$ be the eigenvalues of \mathbf{E} , and \mathbf{q}_1 and \mathbf{q}_2 the corresponding orthonormal eigenvectors. We then define the tensors

$$\mathbf{O}_{11} = \mathbf{q}_1 \otimes \mathbf{q}_1, \quad \mathbf{O}_{22} = \mathbf{q}_2 \otimes \mathbf{q}_2, \quad \mathbf{O}_{12} = \frac{1}{\sqrt{2}}(\mathbf{q}_1 \otimes \mathbf{q}_2 + \mathbf{q}_2 \otimes \mathbf{q}_1),$$

with \otimes the tensor product, and we introduce the following subsets of the space Sym of all symmetric tensors:

$$\begin{aligned} \mathcal{R}_1 &= \{\mathbf{E} \in \text{Sym} \mid \alpha e_1 + 2(1 + \alpha)e_2 < 0\}, \\ \mathcal{R}_2 &= \{\mathbf{E} \in \text{Sym} \mid e_1 > 0\}, \\ \mathcal{R}_3 &= \{\mathbf{E} \in \text{Sym} \mid \alpha e_1 + 2(1 + \alpha)e_2 > 0, e_1 < 0\}, \end{aligned}$$

where $\alpha = \lambda/\mu$. Moreover, we define the interfaces between regions $\mathcal{R}_1, \mathcal{R}_3$ and $\mathcal{R}_2, \mathcal{R}_3$ as

$$\mathcal{I}_{13} = \{\mathbf{E} \in \text{Sym} \mid \alpha e_1 + (2 + \alpha)e_2 = 0\}, \quad \mathcal{I}_{23} = \{\mathbf{E} \in \text{Sym} \mid e_1 = 0\}.$$

As proved in [Lucchesi et al. 1994], if $\mathbf{E} \in \mathcal{R}_1 \cup \mathcal{I}_{13}$, then

$$\mathbf{E}^f = \mathbf{0}, \quad \mathbf{T} = \frac{2\mu}{2 + \alpha} \{ [2(1 + \alpha)e_1 + \alpha e_2] \mathbf{O}_1 + [\alpha e_1 + 2(1 + \alpha)e_2] \mathbf{O}_2 \};$$

if $\mathbf{E} \in \mathcal{R}_2 \cup \mathcal{I}_{23}$, then

$$\mathbf{E}^f = \mathbf{E}, \quad \mathbf{T} = \mathbf{0};$$

and if $\mathbf{E} \in \mathcal{R}_3$, then

$$\mathbf{E}^f = \left[e_2 + \frac{\alpha}{2(1 + \alpha)} e_1 \right] \mathbf{O}_2, \quad \mathbf{T} = \mu \frac{2 + 3\alpha}{1 + \alpha} e_1 \mathbf{O}_1.$$

The derivative $D_E \widehat{\mathbf{T}}(\mathbf{E})$ of $\widehat{\mathbf{T}}$ with respect to \mathbf{E} , which is used for numerical solution of the equilibrium problem (see Section 4), has been explicitly calculated in Lucchesi et al. [1994]. Here, we limit ourselves to recalling its expression. Specifically,

$$D_E \widehat{\mathbf{T}}(\mathbf{E}) = \begin{cases} \mathbb{S}_1 = 2\mu \mathbb{I} + \frac{2\mu\lambda}{2\mu + \lambda} \mathbf{I} \otimes \mathbf{I} & \text{if } \mathbf{E} \in \mathcal{R}_1, \\ \mathbb{S}_2 = \mathbb{O} & \text{if } \mathbf{E} \in \mathcal{R}_2, \\ \mathbb{S}_3 = \frac{\mu(2\mu + 3\lambda)}{\mu + \lambda} (\mathbf{O}_{11} \otimes \mathbf{O}_{11} + \frac{e_1}{e_1 - e_2} \mathbf{O}_{12} \otimes \mathbf{O}_{12}) & \text{if } \mathbf{E} \in \mathcal{R}_3, \end{cases}$$

where \mathbb{I} and \mathbb{O} are the identity and the null fourth-order tensors.

On the interfaces \mathcal{I}_{13} and \mathcal{I}_{23} , the fourth-order tensor $D_E \widehat{\mathbf{T}}(\mathbf{E})$ does not exist. Nevertheless, it can be replaced by suitable convex combinations of \mathbb{S}_3 and \mathbb{S}_1 , and \mathbb{S}_3 and \mathbb{S}_2 , respectively.

\mathbf{E}^f is called the fracture strain because if it is nonnull in any region of the structure, we can expect fractures to be present in that region. Knowing \mathbf{E}^f allows one to get information on the crack distribution. To this end, the vault can be considered constituted by the layers

$$\mathfrak{S}_\zeta = \{\mathbf{p}' \mid \mathbf{p}' = \mathbf{p} + \zeta \mathbf{n}, \mathbf{p} \in \mathfrak{S}, \mathbf{n} = \mathbf{n}(\mathbf{p}), \zeta \in [-h/2, h/2]\}.$$

Assume that in a fixed point \mathbf{p}' belonging to the layer \mathfrak{S}_ζ , one (and only one) eigenvalue of \mathbf{T} is zero, or equivalently, that $\mathbf{E}(\mathbf{p}')$ belongs to the region \mathcal{R}_3 . In this case, \mathbf{E}^f has one eigenvalue that equals zero and one that is positive, and the characteristic direction of the latter coincides with the characteristic

direction corresponding to the null eigenvalue of \mathbf{T} . Then the fractures can open in this direction. Let ε_{11}^f , ε_{22}^f and ε_{12}^f be the components of the fracture strain \mathbf{E}^f with respect to the orthonormal basis $\{\mathbf{g}_1, \mathbf{g}_2\}$. The eigenvalues e_1^f and e_2^f of \mathbf{E}^f have the expressions

$$e_1^f = \frac{\varepsilon_{11}^f + \varepsilon_{22}^f - \sqrt{(\varepsilon_{11}^f - \varepsilon_{22}^f)^2 + 4(\varepsilon_{12}^f)^2}}{2}, \quad e_2^f = \frac{\varepsilon_{11}^f + \varepsilon_{22}^f + \sqrt{(\varepsilon_{11}^f - \varepsilon_{22}^f)^2 + 4(\varepsilon_{12}^f)^2}}{2}.$$

Now assume that $0 = e_1^f < e_2^f$. Since we can limit ourselves to the case of $\varepsilon_{12}^f \neq 0$, the components q_1, q_2 of the eigenvector corresponding to e_2^f satisfy the condition

$$q_2 = (\varepsilon_{22}^f / \varepsilon_{12}^f) q_1.$$

Because $\varepsilon_{22}^f > 0$, we can conclude that as the sign of ε_{12}^f varies, the fractures exhibit the behavior shown in Figure 2. By applying this criterion for each point of the layer \mathfrak{S}_ζ it is possible to draw the corresponding fracture curve.

3. The numerical method

In this section we describe the finite element procedure implemented into the NOSA code for static analysis of masonry vaults and domes. The equilibrium problem of masonry vaults and domes is solved by using quadrilateral eight-node shell elements based on the Love–Kirchhoff hypothesis [Nagtegaal and Slater 1981]. These elements have three degrees of freedom per corner node. The four mid-side nodes have one degree of freedom, namely the rotation around the side. This rotation is independent of the displacements of the corner nodes, and then the elements are nonconforming.

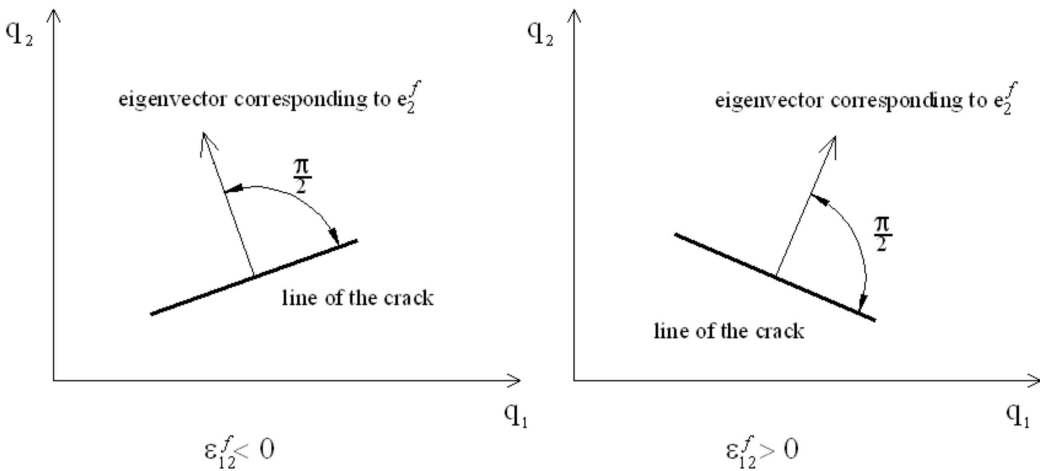


Figure 2. Behavior of the cracks as the sign of ε_{12}^f varies.

The displacements within the element and the rotations are given by

$$\mathbf{u} = \sum_{i=1}^4 \varphi_i \mathbf{u}_i, \quad \theta = \sum_{j=5}^9 \psi_j \theta_j,$$

where \mathbf{u}_i is the displacement vector of the i -th node, φ_i , $i = 1, \dots, 4$ are bilinear shape functions, θ_j , $j = 5, \dots, 8$ are the rotations of the mid-side nodes, θ_9 is the rotation of the centroid, and ψ_j are biquadratic shape functions. We denote by ε_{ij} the component of the total strain with respect to the local basis $\{\mathbf{g}_1, \mathbf{g}_2\}$. The strain vector $\varepsilon = (\varepsilon_{11}, \varepsilon_{22}, \varepsilon_{12})^T$ can be expressed as a function of the generalized displacement vector $\tilde{\mathbf{u}} = (\mathbf{u}_1, \mathbf{u}_2, \mathbf{u}_3, \mathbf{u}_4, \theta_5^s, \theta_6^s, \theta_7^s, \theta_8^s)^T$, where $\theta_5^s, \theta_6^s, \theta_7^s$ and θ_8^s are the rotations of the mid-side nodes around the side itself, via the matrix \mathbf{B} containing the derivatives of the shape functions, $\varepsilon = \mathbf{B}\tilde{\mathbf{u}}$. In particular, matrix \mathbf{B} can be written as

$$\mathbf{B} = [\mathbf{B}^m + \zeta \mathbf{B}^c \quad \zeta \mathbf{B}^\theta] \tag{2}$$

where \mathbf{B}^m accounts for membrane strains, and \mathbf{B}^c and \mathbf{B}^θ account for the curvature changes.

Suitable numerical techniques based on the Newton–Raphson method for solving the nonlinear system obtained by discretizing the structure into finite elements have been developed. To this end, we use the tangent stiffness matrix, whose expression is

$$\mathbf{K}_T = \int_A \int_{-h/2}^{h/2} \mathbf{B}^T \mathbf{D} \mathbf{B} \, d\zeta \, dA, \tag{3}$$

where A is the area of the element and \mathbf{D} is the matrix of the components of the derivative $D_E \widehat{\mathbf{T}}$ of the stress $\widehat{\mathbf{T}}(\mathbf{E})$ with respect to the strain \mathbf{E} , given in Section 2. In view of Equation (2), by means of simple calculations, Equation (3) becomes

$$\mathbf{K}_T = \int_A \begin{bmatrix} \mathbf{B}^{mT} & \mathbf{B}^{cT} \\ \mathbf{0} & \mathbf{B}^{\theta T} \end{bmatrix} \begin{bmatrix} \mathbf{D}_0 & \mathbf{D}_1 \\ \mathbf{D}_1 & \mathbf{D}_2 \end{bmatrix} \begin{bmatrix} \mathbf{B}^m & \mathbf{0} \\ \mathbf{B}^f & \mathbf{B}^\theta \end{bmatrix} dA,$$

where

$$\mathbf{D}_i = \int_{-h/2}^{h/2} \zeta^i \mathbf{D} \, d\zeta, \quad i = 0, 1, 2.$$

4. The maximum modulus eccentricity surface

For each point $\mathbf{p}' = \mathbf{p} + \zeta \mathbf{n}$, with $\mathbf{p} = (\eta_1, \eta_2)$ belonging to the mean surface \mathfrak{S} , we denote by $\mathbf{g}(\gamma) = (\cos \gamma, \sin \gamma)$ the unit tangent vector to \mathfrak{S} at \mathbf{p} , where $\gamma \in [-\pi/2, \pi/2)$ is the angle formed by $\mathbf{g}(\gamma)$ with the direction of η_1 . We set $\sigma(\mathbf{p}, \zeta, \gamma) = \mathbf{g}(\gamma) \cdot \mathbf{T}(\mathbf{p}, \zeta) \mathbf{g}(\gamma)$. Thus, the relations

$$N(\mathbf{p}, \gamma) = \int_{-h/2}^{h/2} \sigma(\mathbf{p}, \zeta, \gamma) \, d\zeta \quad \text{and} \quad M(\mathbf{p}, \gamma) = \int_{-h/2}^{h/2} \sigma(\mathbf{p}, \zeta, \gamma) \zeta \, d\zeta$$

define the normal force and the bending moment per unit length corresponding to $\mathbf{g}(\gamma)$, respectively. In view of the fact that $\mathbf{T}(\mathbf{p}, \zeta)$ is negative semidefinite, $N(\mathbf{p}, \gamma)$ is nonpositive for every γ . Moreover,

$$|M(\mathbf{p}, \gamma)| = \left| \int_{-h/2}^{h/2} \sigma(\mathbf{p}, \zeta, \gamma) \zeta \, d\zeta \right| \leq \int_{-h/2}^{h/2} |\sigma(\mathbf{p}, \zeta, \gamma) \zeta| \, d\zeta \leq \frac{h}{2} |N(\mathbf{p}, \gamma)|, \quad (4)$$

where the next to last step is justified by the fact that $\sigma(\mathbf{p}, \zeta, \gamma) \leq 0$ for each γ and ζ .

We denote by $\mathbf{M}(\mathbf{p})$ and $\mathbf{N}(\mathbf{p})$ the tensors defined by

$$\mathbf{M}(\mathbf{p}) = \int_{-h/2}^{h/2} \mathbf{T}(\mathbf{p}, \zeta) \zeta \, d\zeta, \quad \mathbf{N}(\mathbf{p}) = \int_{-h/2}^{h/2} \mathbf{T}(\mathbf{p}, \zeta) \, d\zeta.$$

Since

$$M(\mathbf{p}, \gamma) = \mathbf{g}(\gamma) \cdot \mathbf{M}(\mathbf{p}) \mathbf{g}(\gamma), \quad N(\mathbf{p}, \gamma) = \mathbf{g}(\gamma) \cdot \mathbf{N}(\mathbf{p}) \mathbf{g}(\gamma), \quad (5)$$

it is a simple matter to show that inequality in Equation (4) is equivalent to the conditions

$$\mathbf{g}(\gamma) \cdot (\mathbf{M}(\mathbf{p}) - \frac{1}{2}h\mathbf{N}(\mathbf{p})) \mathbf{g}(\gamma) \geq 0, \quad \mathbf{g}(\gamma) \cdot (\mathbf{M}(\mathbf{p}) + \frac{1}{2}h\mathbf{N}(\mathbf{p})) \mathbf{g}(\gamma) \leq 0, \quad (6)$$

which in turn, express the positive and negative semidefiniteness of $\mathbf{M}(\mathbf{p}) - \frac{1}{2}h\mathbf{N}(\mathbf{p})$ and $\mathbf{M}(\mathbf{p}) + \frac{1}{2}h\mathbf{N}(\mathbf{p})$. Now let us exclude that the normal force may be zero in all directions at any point of the vault. For each $\gamma \in [-\pi/2, \pi/2)$, let us define the corresponding eccentricity

$$e(\mathbf{p}, \gamma) = \frac{M(\mathbf{p}, \gamma)}{N(\mathbf{p}, \gamma)}. \quad (7)$$

The function $e(\mathbf{p}, \gamma)$ is well-defined and continuous whenever $N(\mathbf{p}, \gamma) \neq 0$. Moreover, if there exists γ_1 such that $N(\mathbf{p}, \gamma_1) = 0$, then $e(\mathbf{p}, \gamma)$ is a constant function of γ . In fact, we start by observing that if $N(\mathbf{p}, \gamma_1) = 0$, then, from the negative semidefiniteness of $\mathbf{N}(\mathbf{p})$, the relation $\mathbf{N}(\mathbf{p}) \mathbf{g}(\gamma_1) = \mathbf{0}$ follows. Moreover, using the preceding relation in Equation (6), we arrive at $\mathbf{M}(\mathbf{p}) \mathbf{g}(\gamma_1) = \mathbf{0}$. Then, a vector $\mathbf{g}(\gamma_2)$ orthogonal to $\mathbf{g}(\gamma_1)$ is a common eigenvector of $\mathbf{M}(\mathbf{p})$ and $\mathbf{N}(\mathbf{p})$. Denote by m and $n < 0$ the corresponding eigenvalues. Setting $\mathbf{g}(\gamma) = \beta_1 \mathbf{g}(\gamma_1) + \beta_2 \mathbf{g}(\gamma_2)$, with $\beta_1^2 + \beta_2^2 = 1$, we obtain

$$e(\mathbf{p}, \gamma) = \frac{(\beta_1 \mathbf{g}(\gamma_1) + \beta_2 \mathbf{g}(\gamma_2)) \cdot \mathbf{M}(\mathbf{p}) (\beta_2 \mathbf{g}(\gamma_2))}{(\beta_1 \mathbf{g}(\gamma_1) + \beta_2 \mathbf{g}(\gamma_2)) \cdot \mathbf{N}(\mathbf{p}) (\beta_2 \mathbf{g}(\gamma_2))} = \frac{m}{n}, \quad (8)$$

and thus $e(\mathbf{p}, \gamma)$ does not depend on γ .

For each point \mathbf{p} of the mean surface, let $\gamma_0 \in [-\pi/2, \pi/2)$ be the value of γ (not necessarily unique) for which the function $|e(\mathbf{p}, \gamma)| = |M(\mathbf{p}, \gamma)/N(\mathbf{p}, \gamma)|$ reaches its maximum value. The quantity

$$\tilde{e}(\mathbf{p}) = \frac{M(\mathbf{p}, \gamma_0)}{N(\mathbf{p}, \gamma_0)}$$

is the maximum modulus eccentricity at point \mathbf{p} . The surface

$$\mathfrak{M} = \{\mathbf{p}' \mid \mathbf{p}' = \mathbf{p} + \tilde{e}(\mathbf{p}) \mathbf{n}, \mathbf{p} \in \mathfrak{S}, \mathbf{n} = \mathbf{n}(\mathbf{p})\}, \quad (9)$$

obtained by translating points \mathbf{p} belonging to \mathfrak{S} by the value $\tilde{e}(\mathbf{p})$ along the unit normal vector \mathbf{n} to \mathfrak{S} , is the maximum modulus eccentricity surface (m.m.e.s.). The only points \mathbf{p} where \mathfrak{M} is not defined are those for which two values γ_0 and γ_1 exist that maximize the function $|e(\mathbf{p}, \gamma)|$ with $e(\mathbf{p}, \gamma_0) = -e(\mathbf{p}, \gamma_1)$.

In the particular case in which the vault’s geometry and loads possess axial symmetry, then the eccentricity can attain its maximum modulus only in the direction of parallels or meridians [Lucchesi et al. 1999]. Note that, in view of inequality in Equation (4), the m.m.e.s. corresponding to a negative semidefinite stress field is entirely contained within the vault.

With the aim of determining the maximum and the minimum of function $e(\mathbf{p}, \gamma)$, as γ varies in $[-\pi/2, \pi/2)$, we can limit ourselves to the case in which $\det \mathbf{N}(\mathbf{p}) \neq 0$ (see Equation (8)). In fact, as already pointed out, if $\det \mathbf{N}(\mathbf{p}) = 0$, then $e(\mathbf{p}, \gamma)$ is the constant function m/n . Due to Equations (5) and (7) the quantity $e(\mathbf{p}, \gamma)$ is the Rayleigh quotient corresponding to the generalized eigenvalue problem $\mathbf{M}(\mathbf{p})\mathbf{f} = \omega\mathbf{N}(\mathbf{p})\mathbf{f}$, whose eigenvalues are¹

$$\omega_1 = \frac{\text{tr}(\mathbf{N}^{-1}\mathbf{M})(\det \mathbf{N}) - \sqrt{(\text{tr}(\mathbf{N}^{-1}\mathbf{M}))^2(\det \mathbf{N})^2 - 4 \det \mathbf{N} \det \mathbf{M}}}{2 \det \mathbf{N}},$$

$$\omega_2 = \frac{\text{tr}(\mathbf{N}^{-1}\mathbf{M})(\det \mathbf{N}) + \sqrt{(\text{tr}(\mathbf{N}^{-1}\mathbf{M}))^2(\det \mathbf{N})^2 - 4 \det \mathbf{N} \det \mathbf{M}}}{2 \det \mathbf{N}},$$

with eigenvectors \mathbf{f}_1 and \mathbf{f}_2 . It is well known that the Rayleigh quotient $e(\mathbf{p}, \gamma)$ belongs to the interval $[\omega_1, \omega_2]$; thus, we can conclude that the minimum and the maximum of $e(\mathbf{p}, \gamma)$ are ω_1 and ω_2 . Finally,

$$\tilde{e}(\mathbf{p}) = \begin{cases} \omega_1 & \text{if } \det \mathbf{N}(\mathbf{p}) \neq 0, |\omega_1| \geq |\omega_2|, \\ \omega_2 & \text{if } \det \mathbf{N}(\mathbf{p}) \neq 0, |\omega_1| \leq |\omega_2|, \\ m/n & \text{if } \det \mathbf{N}(\mathbf{p}) = 0. \end{cases}$$

If the m.m.e.s. is tangent to the extrados or intrados along a path, such a path can be considered the site of cylindrical hinges. The corresponding rotational axis coincides with the direction orthogonal to the direction for which the absolute value of the eccentricity is maximum. Therefore, under the hypothesis that the masonry has infinite compressive strength and sliding failure cannot occur, as the load increases, vault collapse occurs when the m.m.e.s. is tangent to the intrados or extrados along paths, in such a way as to determine a hinge distribution sufficient to render the vault a kinematically undetermined structure. It should be pointed out that in the model presented herein, collapse of a masonry vault is due to the formation of hinges on its extrados and intrados. However, other collapse mechanisms can be considered, for example by removing the “non-sliding” assumption [Livesley 1978] or assuming a bounded compressive strength for the masonry [Livesley 1992a].

Knowing \tilde{e} at each point of the mean surface allows for defining some “geometrical” factors of safety. By following the suggestion of Heyman [1982], for each $\mathbf{p} \in \mathfrak{S}$ we put

$$\bar{h}(\mathbf{p}) = \begin{cases} \omega_2 - \omega_1 & \text{if } \det \mathbf{N}(\mathbf{p}) \neq 0, \\ 2|m/n| & \text{if } \det \mathbf{N}(\mathbf{p}) = 0. \end{cases}$$

¹The expression for these same quantities presented in [Lucchesi et al. 1999] contained errors which are corrected here.

We determine $v = \int_{\mathfrak{S}} \bar{h}(\mathbf{p}) \, da$, which is the volume of the smallest vault able to contain the m.m.e.s. Then we determine the volume V of the vault and set

$$\varphi_v = \frac{V - v}{V} = 1 - \frac{v}{V}. \quad (10)$$

Alternatively, we can put

$$\bar{e} = \sup_{\mathbf{p} \in \mathfrak{S}} \frac{2 |\tilde{e}(\mathbf{p})|}{h(\mathbf{p})}, \quad (11)$$

where $h(\mathbf{p})$ is the thickness of the vault, and consider

$$\varphi_s = 1 - \bar{e}. \quad (12)$$

The coefficient φ_s can turn out to be very conservative. In fact, in view of the definition in Equation (11), the presence of a single point at which the m.m.e.s. comes close to the boundary of the vault causes φ_s to approach zero.

5. Examples

This section is aimed at assessing the effectiveness of the method proposed in the paper and implemented in the finite element code NOSA. Three example applications are addressed. The first two applications deal with the limit analysis of simple masonry structures. We determine the collapse load and the collapse mechanism for a circular plate subjected to a lateral pressure and an increasing vertical force. Then, we study a spherical vault subjected to its own weight and a point load applied at the keystone. For both cases, we determine the exact solution and then, for the sake of comparison, conduct a finite element analysis by increasing the variable load until it is no longer possible to find an admissible (that is, negative semidefinite at each point of the structure) equilibrated stress field. The reader is referred to [Del Piero 1998] for a general treatment of the limit analysis of masonry-like materials and to [Lucchesi et al. 1999] for the definitions and the results concerning the limit analysis of masonry vaults. Last, we describe the study conducted via the NOSA code on the dome and the drum of the Church of Santa Maria Maddalena in Morano Calabro. We analyzed the behavior of the structure subjected to its own weight as well as in the presence of settlements of the base of the drum.

5.1. The circular plate. In the cylindrical reference system $\{\mathbf{O}, r, \theta, z\}$, consider the circular plate \mathcal{P} with radius R and thickness h , constrained along the lateral surface $\{r = R\}$ in such a way that rotation and vertical displacements are prevented (Figure 3). The plate is subjected to a horizontal pressure \mathbf{c}_0 , uniformly distributed on the lateral surface, and a vertical pressure $\lambda \mathbf{c}_1$, uniformly distributed on the circle of the extrados $0 \leq r \leq b$, with $b \leq R$. For the sake of simplicity, we have ignored weight, but the corresponding generalization presents no difficulties.

We aim to determine the collapse multiplier λ_c . To this end, for $\lambda > 0$ we determine an admissible internal forces field equilibrated with the load $\mathbf{c}_0 + \lambda \mathbf{c}_1$ and then find the multiplier $\lambda = \lambda_c$, such that there is a collapse mechanism corresponding to the internal forces equilibrated with $\mathbf{c}_0 + \lambda_c \mathbf{c}_1$ [Lucchesi et al. 1999]. Let Q , N_r , N_θ , M_r and M_θ be respectively the shear, radial and circumferential normal forces, and the radial and circumferential bending moment per unit length. They must satisfy the equilibrium

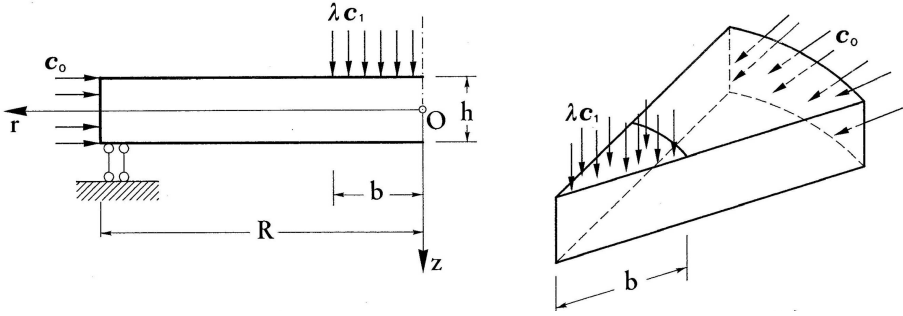


Figure 3. The circular plate.

equations [Timoshenko and Woinowsky-Krieger 1987]

$$\frac{dQ}{dr} + \frac{1}{r}Q = \lambda c_1, \tag{13}$$

$$\frac{dN_r}{dr} + \frac{1}{r}N_r - \frac{1}{r}N_\theta = 0, \tag{14}$$

$$\frac{dM_r}{dr} + \frac{1}{r}M_r - \frac{1}{r}M_\theta + Q = 0, \tag{15}$$

where

$$c_1(r) = \begin{cases} 1 & \text{if } 0 \leq r \leq b, \\ 0 & \text{if } b < r \leq R, \end{cases} \tag{16}$$

and the boundary conditions

$$Q(R) = \frac{\lambda b^2}{2R}, \quad N_r(R) = -c_0 h, \quad c_0 = |c_0|. \tag{17}$$

Since the internal forces to be determined must be collapse internal forces, by setting $e_r = M_r/N_r$, $e_\theta = M_\theta/N_\theta$, we require that they satisfy the further boundary conditions

$$e_r(0) = -\frac{h}{2}, \quad e_r(R) = \frac{h}{2}, \tag{18}$$

and that the equality

$$e_\theta(r) = -\frac{h}{2} \tag{19}$$

holds for $0 \leq r \leq R$. Finally, in order for internal forces to be admissible, we require that the inequalities

$$N_r(r) \leq 0, \quad N_\theta(r) \leq 0, \quad -\frac{h}{2} \leq e_r(r) \leq \frac{h}{2} \tag{20}$$

be satisfied for $0 \leq r \leq R$.

From Equations (13), (16) and (17) we can immediately deduce the shear:

$$Q(r) = \begin{cases} \lambda r/2 & \text{if } 0 \leq r \leq b, \\ \lambda b^2/(2r) & \text{if } b < r \leq R. \end{cases}$$

Equations (14), (15) and (19) are insufficient to determine the remaining four internal forces. A further condition is needed. This condition is obtained by assuming the circumferential normal force to be constant, $N_\theta(r) = \kappa$ for $0 \leq r \leq R$, with $\kappa \leq 0$. From Equation (19) we then deduce $M_\theta(r) = -\frac{1}{2}h\kappa$ for $0 \leq r \leq R$. By integrating Equation (14) with the help of Equation (17)₂, we obtain

$$N_r(r) = -\frac{R}{r}(c_0h + \kappa) + \kappa,$$

and from the admissibility conditions in (20)₁ and (20)₂, we obtain $-c_0h \leq \kappa \leq 0$. Lastly, by integrating Equation (15) with boundary condition (18)₁, we arrive at the expression of M_r which depends on λ . The boundary condition (18)₂ is satisfied for $\lambda = \lambda_c$ with

$$\lambda_c = \frac{6c_0Rh^2}{b^2(3R - 2b)}. \quad (21)$$

It, in turn, allows for determining the final expression for M_r ,

$$M_r(r) = \begin{cases} \frac{1}{2r} \left(hR(c_0h + \kappa) - h\kappa r - \frac{2c_0h^2R}{b^2(3R - 2b)}r^3 \right) & \text{if } 0 < r \leq b, \\ \frac{1}{2r} \left(hR(c_0h + \kappa) - h\kappa r - \frac{2c_0h^2b^2R}{(3R - 2b)^3}(3r - 2b) \right) & \text{if } b \leq r \leq R. \end{cases}$$

It is a simple matter to verify that the admissibility condition in Equation (20)₃ is satisfied.

In view of Equations (18) and (19), the m.m.e.s. corresponding to the determined internal forces is a plane region coinciding with the extrados for $0 \leq r < R$ and undefined for $r = R$. In fact, for $0 \leq r \leq R$ the eccentricity e_θ is $-\frac{1}{2}h$, and the absolute value of the radial eccentricity e_r is less than $\frac{1}{2}h$. For $r = R$, we have $e_r = \frac{1}{2}h$.

The value of λ_c given by Equation (21) is the collapse multiplier. In fact, the displacement field suggested by the shape of the m.m.e.s. and shown in Figure 4 is a collapse mechanism. Each section $\theta = \text{constant}$ rotates around the absolute center of rotation P of the extrados. This rotation is possible because, in view of Equation (18)₂, the sliding clamp shown in Figure 3 has released as depicted in Figure 4, left. From Equation (19) it follows that each radius of the extrados is the axis of a cylindrical hinge. These hinges allow the surface of the extrados to form the lateral surface of a cone; see Figure 4, right.

One quarter of the plate, with $R = 0.5$ m and $h = 0.01$ m has been discretized and analyzed via the finite element code NOSA. After applying the horizontal pressure $c_0 = 5 \cdot 10^4$ Pa, the vertical pressure λ , uniformly distributed throughout the extrados ($b = R$), is progressively increased by assigning successive load increments until convergence can be reached. By using the stress field corresponding to the last load increment, the maximum modulus eccentricity surface has been determined. (In Figure 5 the thickness of the plate has been magnified ten times in order to better illustrate the surface.)

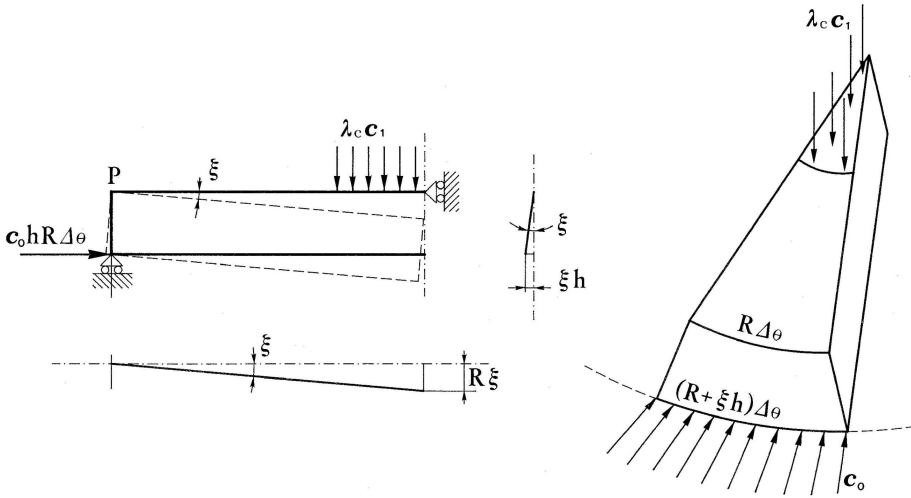


Figure 4. The plate collapse mechanism.

For the numerical example presented here, relation (21) with $b = R$ yields $\lambda_c = 6c_0h^2/R^2 = 120$ Pa. Naturally, the value of λ_s of the pressure beyond which it is impossible to obtain a numerical solution to the plate equilibrium problem depends on the refinement of the mesh and the entity of the load increments. More precisely, we have verified that, for an assigned load increment, using a less refined mesh yields a higher value of λ_s . For example, with 900 and 4000 elements, we get $\lambda_s = 125.8$ Pa and $\lambda_s = 120$ Pa, respectively.

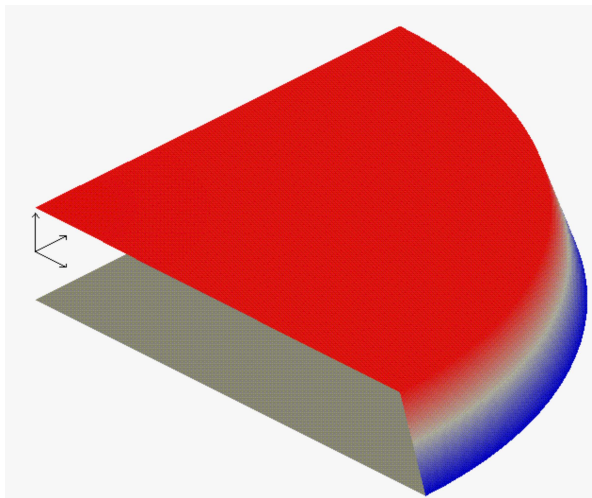


Figure 5. The m.m.e.s. at the instant of collapse.

5.2. The spherical dome. In the spherical reference system $\{O, r, \theta, \varphi\}$, consider the spherical vault \mathcal{D} , with mean radius R and thickness h . The vault is clamped at the springings and subjected to its own weight \mathbf{c}_0 and a point load $\lambda \mathbf{c}_1$ applied at the keystone. Our aim is to determine the value of the collapse multiplier λ_c .

We begin by writing the equilibrium equations for the dome under the assumption that the circumferential normal force and bending moment vanish. Denoting q as the weight of the vault per unit area, N and M as the meridional normal force and bending moment per unit length, respectively, and Q as the shear per unit length, we can write (see [Timoshenko and Woinowsky-Krieger 1987])

$$\frac{d\bar{N}(\varphi)}{d\varphi} - \bar{Q}(\varphi) + Rq \sin^2 \varphi = 0, \quad (22)$$

$$\frac{d\bar{Q}(\varphi)}{d\varphi} + \bar{N}(\varphi) + Rq \sin \varphi \cos \varphi = 0, \quad (23)$$

$$\frac{d\bar{M}(\varphi)}{d\varphi} - R\bar{Q}(\varphi) = 0, \quad (24)$$

where $\bar{N}(\varphi) = N(\varphi) \sin \varphi$, $\bar{Q}(\varphi) = Q(\varphi) \sin \varphi$, $\bar{M}(\varphi) = M(\varphi) \sin \varphi$. Moreover, by imposing vertical force equilibrium of the spherical bowl with amplitude φ we obtain

$$2\pi R\bar{N}(\varphi) + 2\pi R\bar{Q}(\varphi) \cos \varphi + T(\varphi) = 0, \quad (25)$$

where $T(\varphi) = 2\pi R^2 q(1 - \cos \varphi) + \lambda$ is the total load acting on the spherical bowl. By taking $\bar{Q}(\varphi)$ from Equation (25) and substituting into Equation (22), we get

$$\frac{d\bar{N}(\varphi)}{d\varphi} + \bar{N}(\varphi) \tan \varphi + \frac{Rq(p - \cos^3 \varphi)}{\cos \varphi} = 0, \quad (26)$$

where we have put

$$p = 1 + \frac{\lambda}{2\pi R^2 q}, \quad p \geq 1. \quad (27)$$

The solution to Equation (26) in the interval $[0, \pi/2]$ is $\bar{N}(\varphi) = \bar{N}(0) \cos \varphi + Rq \sin \varphi (\cos \varphi - p)$. On the other hand, by imposing horizontal force equilibrium of a slice of amplitude $\Delta\theta$, we obtain $R\Delta\theta[\bar{N}(0) + \bar{Q}(\pi/2)] = 0$, from which we deduce $\bar{N}(0) = -\bar{Q}(\pi/2) \cos \varphi + Rq \sin \varphi (\cos \varphi - p)$. From the above relation, with the help of Equation (25) we can easily derive the expression for shear, $\bar{Q}(\varphi) = -\bar{Q}(\pi/2) - Rq \cos \varphi (p - \cos \varphi)$. As $\bar{Q}(\varphi)$ is now known, we can integrate Equation (24), obtaining

$$\bar{M}(\varphi) = \frac{\pi}{2} (\bar{M} - R\bar{Q} \cos \varphi) + qR^2 \left(\frac{2\varphi - \pi + \sin 2\varphi}{4} + p(1 - \sin \varphi) \right). \quad (28)$$

Since we are interested in determining collapse internal forces, we assume that two hinges form at the extrados, one at the crown and the other at the springing,

$$e(0) = \frac{\bar{M}(0)}{\bar{N}(0)} = -\frac{h}{2}, \quad e(\pi/2) = \frac{\bar{M}(\pi/2)}{\bar{N}(\pi/2)} = -\frac{h}{2}. \quad (29)$$

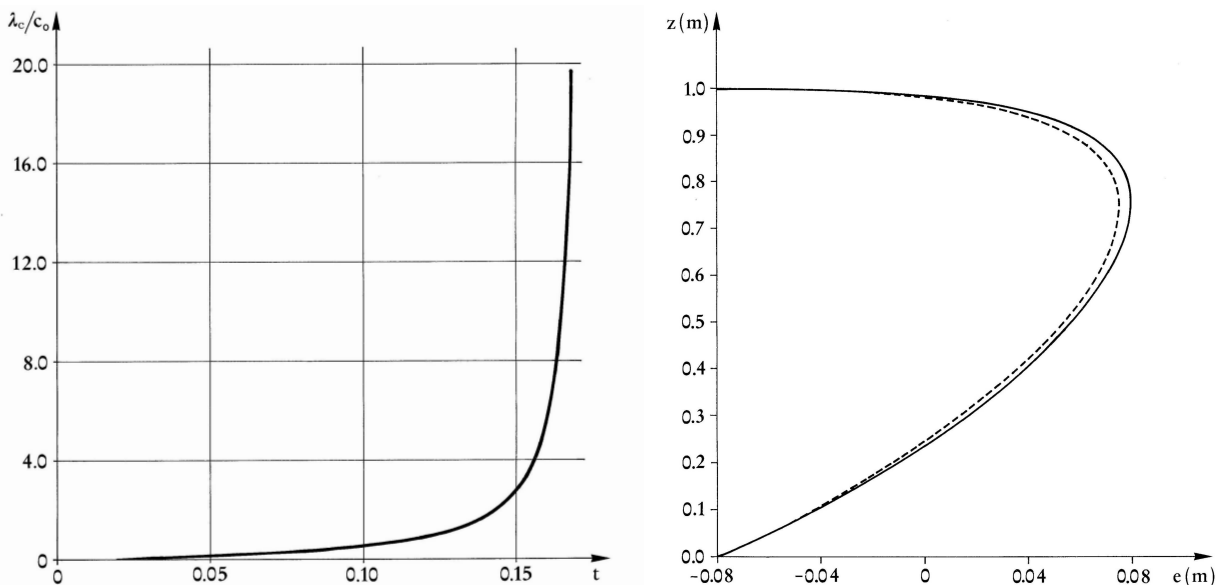


Figure 7. Left: λ_c/c_0 as a function of t . Right: Eccentricity e as a function of $z = R \cos \varphi$ at collapse.

(27)), it is sufficient to determine a corresponding mechanism. Figure 6 suggests considering the vault to be a kinematically undetermined structure made up of slices of infinitesimal amplitude, each in turn constituted by two bodies $\{0 \leq \varphi \leq \bar{\varphi}\}$ and $\{\bar{\varphi} \leq \varphi \leq \pi/2\}$ linked by the hinge at point C . The absolute centers of rotation of the first and second body are the points A and B , respectively. Figure 7, left, shows the behavior of the ratio λ_c/c_0 as a function of $t = h/(2R)$. In particular, $h \approx 0.0377 R$ is the minimum thickness necessary for the vault to be in equilibrium with its own weight. Moreover, as t approaches the value of about 0.17, the collapse load grows infinitely.

One quarter-vault with $R = 1$ m, $h = 0.16$ m and specific weight 20000 N/m³ has been discretized with 3200 shell elements and analyzed with the NOSA code. The load multiplier λ is increased incrementally up to the value λ_s beyond which it is no longer possible to obtain convergence. For the case at hand, the collapse multiplier is $\lambda_c = 6230$ N and the collapse load calculated by NOSA is $\lambda_s = 6200$ N. Figure 7, right, shows a comparison of the eccentricity derived from the stress field calculated numerically at the instant of collapse (dotted line) with the eccentricity obtained from Equation (31) (continuous line).

5.3. The dome of the Church of S. Maria Maddalena in Morano Calabro. Historical information on the church and the operations to which it has been subjected over the centuries is quite scarce. It was probably built during the Middle Ages on top of an earlier chapel situated outside the town. It was enlarged and restored in the sixteenth and eighteenth centuries.

As for the structural layout, the church is a load bearing masonry building in a Latin cross plan, with a central nave and two side aisles. The church is about 50 m long, 24 m wide and 33 m high; see Figure 8. The presbytery zone is delimited by an octagonal cross-section drum supporting a dome and a lantern. The drum has a diameter of about 11 m, height of 6.10 m and constant thickness of 110 cm. The 8 m-high dome has a diameter equal to that of the drum and thickness varying from 110 cm at the springing to

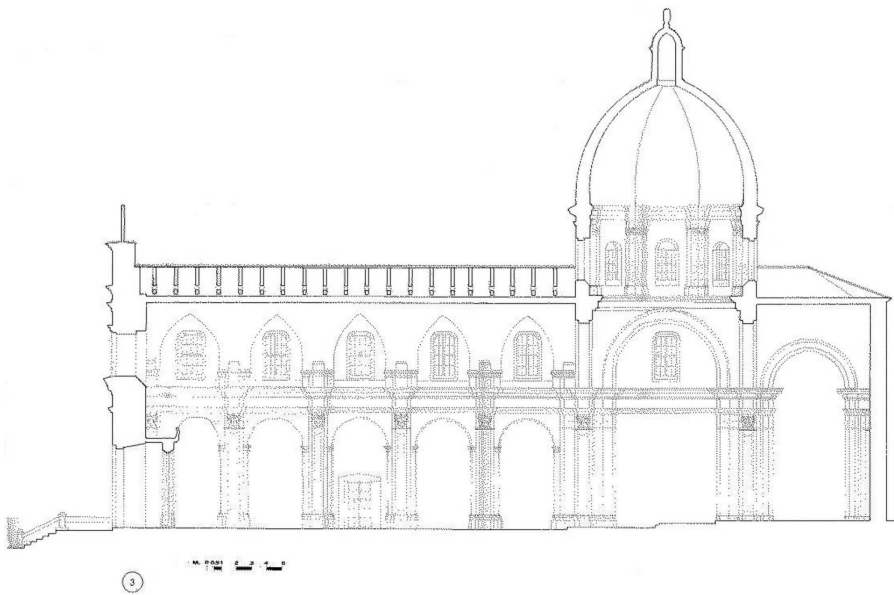


Figure 8. Longitudinal section of the church by the nave.

70 cm at its top. Here, there is a lantern with diameter of 2 m, height of 3.4 m and thickness of about 40 cm.

A survey of the cracking and its distribution in both the drum and dome was carried out in October 2004. In the dome, the crack distribution is known only for the intrados, because the extrados is completely covered with majolica tiles. The dome shows widespread cracking, as well as evident signs of water seepage. The intrados bears two sets of fractures, different in both dimensions and behavior. The first

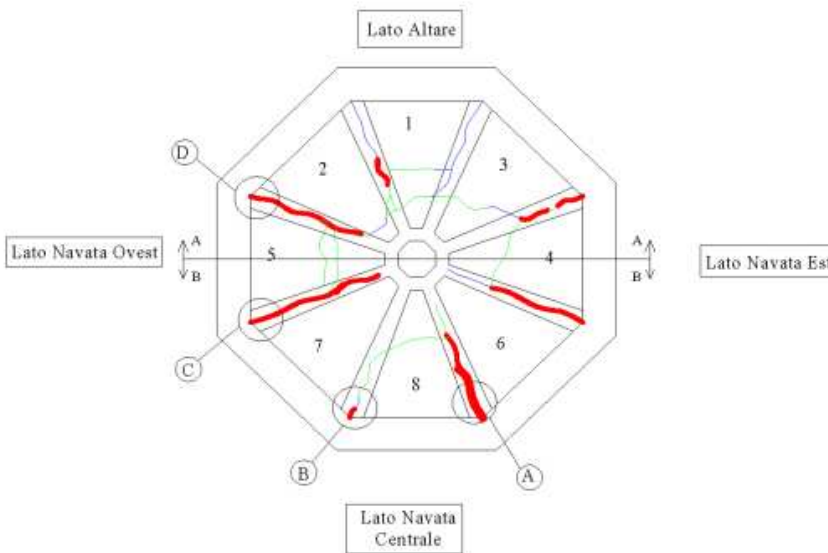


Figure 9. Distribution of cracks in the intrados of the dome.

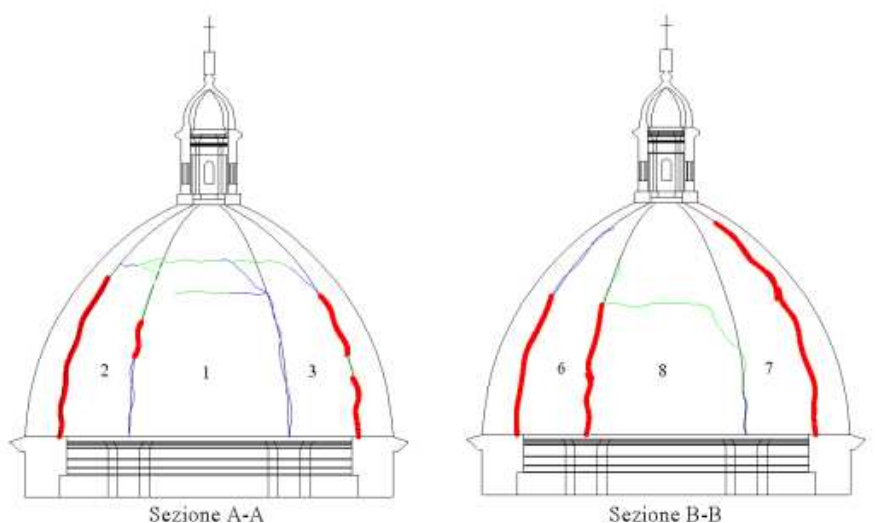


Figure 10. Sections A-A and B-B of the dome: crack distribution in the intrados.

set, which contains the larger cracks, involves the ribs connecting the webs of the dome. These cracks extend from the top of the drum up to well beyond the mid-height of the dome (Figures 9 and 10). The width of the cracks is maximum in correspondence to the dome base and decreases towards its top, where the cracks close and do not affect the last part of the ribs. The second set of cracks is horizontal and located in the webs, in the upper half of the dome. They extend from one rib to the next, inscribing a closed circular curve which involves nearly the entire dome. The width of these openings is much smaller than the first, vertical set of cracks. Rather, the drum is in relatively good condition; the survey revealed the presence of a few cracks with moderate extension. In particular, the cracks are located at the top of the drum and are continuations of those on the dome. They extend onto the drum for a short stretch and stop above the windows.

The crack survey of the structure is shown in Figures 9 and 10, where different colors are used to represent fractures with different width: red, blue and green represent cracks of major, medium and minor width, respectively.

Finite-element structural analyses of the dome as well as the drum have been performed with NOSA. The structure was discretized with 5496 shell elements (Figure 11, left). At first, the base of the drum was considered to be clamped and the effects of the other parts of the church thereby neglected. Further analyses were then carried out with the aim of assessing the effects of vertical settlements of the drum. Since no experimental data are available for the masonry material of the structure, we assumed $\gamma = 20000 \text{ N/m}^3$ for the specific weight, $E = 3.0 \times 10^9 \text{ Pa}$ for the Young's modulus and $\nu = 0.1$ for the Poisson's ratio.

In the following we describe the results of the analysis of the structure subjected to its own weight. Maximum horizontal displacement values of about 1.9 mm are reached at the base of the dome. The maximum vertical displacements, of about 1.6 mm, occur in the lantern and on the top of the dome.

A global analysis of the entire structure allows for concluding that compressive stresses are less than $13 \times 10^5 \text{ Pa}$, a value considered acceptable. Figure 11, right, illustrates the m.m.e.s. for a web together

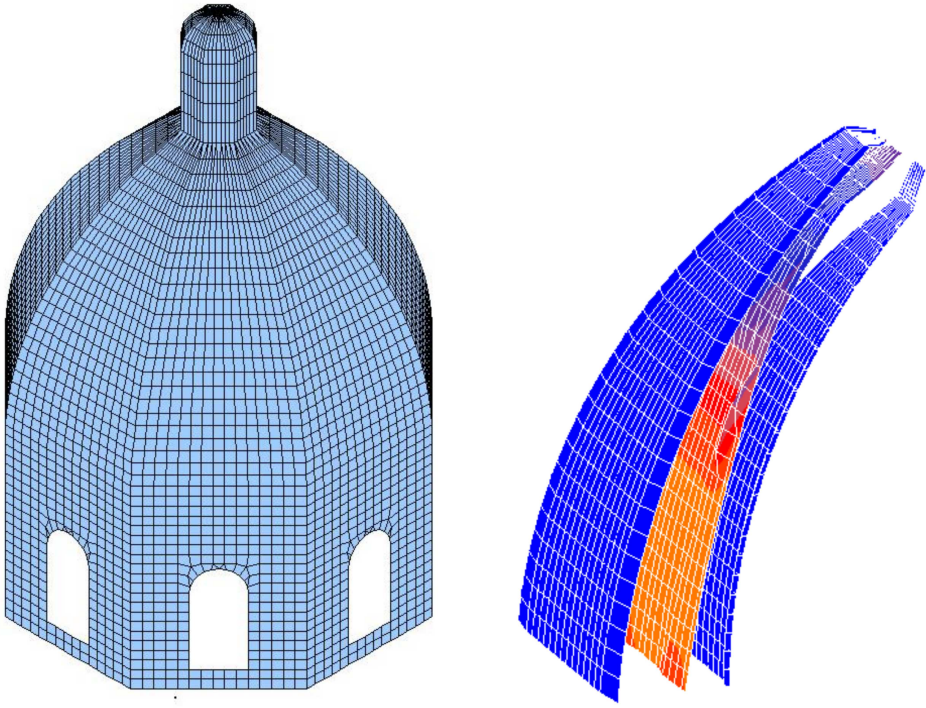


Figure 11. Left: Finite element discretization of the dome and the drum. Right: Maximum modulus eccentricity surface in a web.

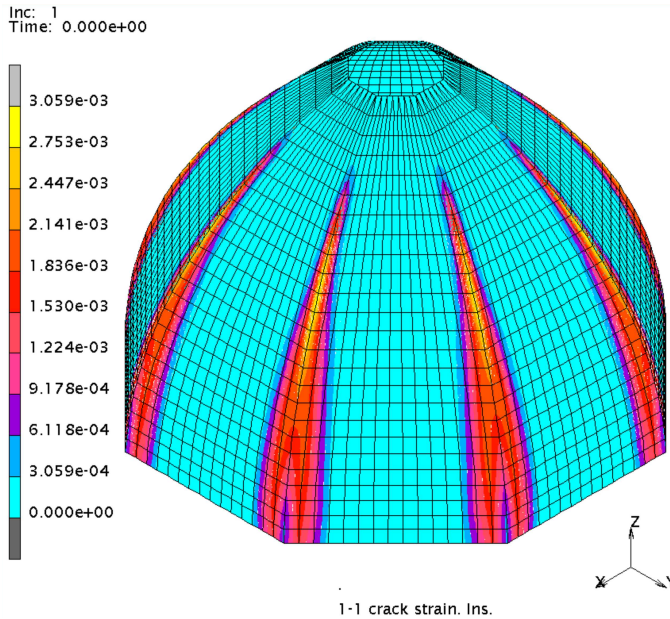


Figure 12. Component ε_{11}^f of the fracture strain at the intrados of the dome subjected to its own weight.

with the extrados and the intrados (in blue). As for the intrados, it is in agreement with the crack distribution shown in Figures 9 and 10. Moreover, as for the factors defined in Equations (10) and (12), we have $\varphi_v = 0.71$ and $\varphi_s = 0.17$.

With the aim of determining the direction of any eventual cracking, the components of the fracture strain in correspondence to both the intrados and the extrados were analyzed. Let

$$\varepsilon_{11}^f(\mathbf{p}, \zeta) = \mathbf{g}_1 \mathbf{E}^f(\mathbf{p}, \zeta) \mathbf{g}_1 \quad \text{and} \quad \varepsilon_{22}^f(\mathbf{p}, \zeta) = \mathbf{g}_2 \mathbf{E}^f(\mathbf{p}, \zeta) \mathbf{g}_2$$

be the components of the fracture strain along parallels and meridians, respectively, and

$$\varepsilon_{12}^f(\mathbf{p}, \zeta) = \mathbf{g}_1 \mathbf{E}^f(\mathbf{p}, \zeta) \mathbf{g}_2$$

be the shear component. The behavior of ε_{11}^f , ε_{22}^f , ε_{12}^f is shown in Figures 12–14 for the dome. For ε_{11}^f , the highest values are reached in the ribs starting at the top of the drum and continuing up to a certain height. In these regions ε_{22}^f and ε_{12}^f are equal to zero, which leads to the conclusion that there are fractures along the meridians, concentrated in the ribs. These fractures start at the base of the dome, reach a certain height and then close. On the lower part, they continue downward, past the dome onto the upper portion of the drum. The ε_{22}^f component reaches its maximum value in the upper half of the dome, at about 6.90 m from the springing, in the center of the webs, where ε_{11}^f and ε_{12}^f are negligible. We deduce that in these regions the fractures have the same directions as parallels of latitude. Moreover, near the ribs, ε_{11}^f , ε_{22}^f and ε_{12}^f are nonzero and the parallels are no longer principal directions for the fracture strain. By applying the criterion described in Section 2 (see Figure 2) we deduce that here the fractures join the ribs, arranged so as to form an approximate upside down U shape (see Figure 9).

As for the extrados, the numerical results suggest the presence of fracturing along the ribs, higher up than that on the intrados. Over the base of the dome, at about 2 m from the springing, there is another series of fractures similar to those on the intrados: they follow the parallel in the central part of each web and join the ribs, with a similar upside down U trend.

The agreement between the crack distribution actually observed in the intrados and the numerical results obtained confirms the effectiveness of the finite-element code NOSA and represents substantial grounds for considering the results obtained for the dome extrados as realistic and reliable as well.

Further numerical analyses were conducted with the aim of assessing the behavior of the structure in the presence of vertical settlements of the base of the drum. These investigations can be useful to explain the origin of the asymmetries of the crack distribution seen in Figures 9 and 10. To model sinking of the foundations, three adjacent sides of the base of the drum are subjected to a vertical piecewise linear displacement. In particular, we imposed a constant displacement of 1 cm to the central side, and a linear displacement varying from 1 to 0 to the other two sides. A displacement of the same kind has been assigned to the other three opposite sides, with a maximum displacement of 0.5 cm. In this case compressive stresses are less than 18×10^5 Pa. As for the factors of safety, the worst condition occurs in webs 3 and 7, where we have $\varphi_v = 0.46$ and $\varphi_s = 0$. Figures 15–17 show the components ε_{11}^f , ε_{22}^f and ε_{12}^f in the intrados of the dome. We point out that due to the assigned vertical displacement, no new fractures form in addition to those corresponding to the weight, and they rearrange in an asymmetric way, in agreement with Figures 9 and 10.

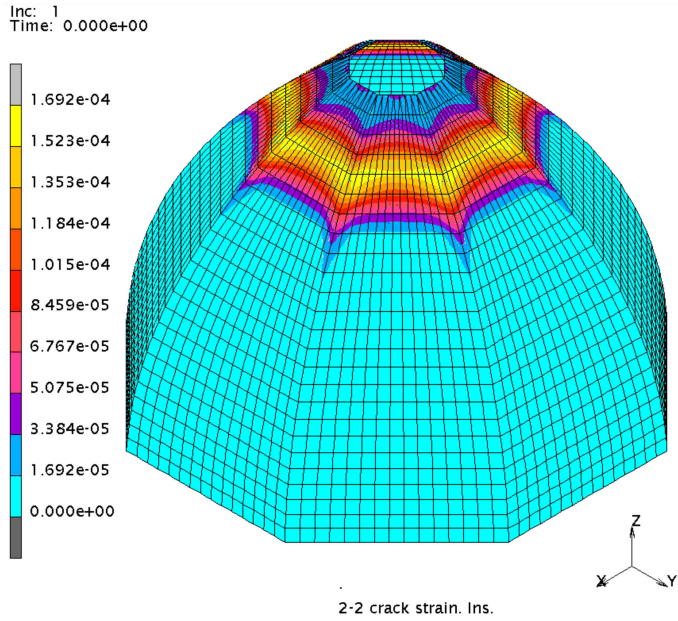


Figure 13. Component ε_{22}^f of the fracture strain at the intrados of the dome subjected to its own weight.

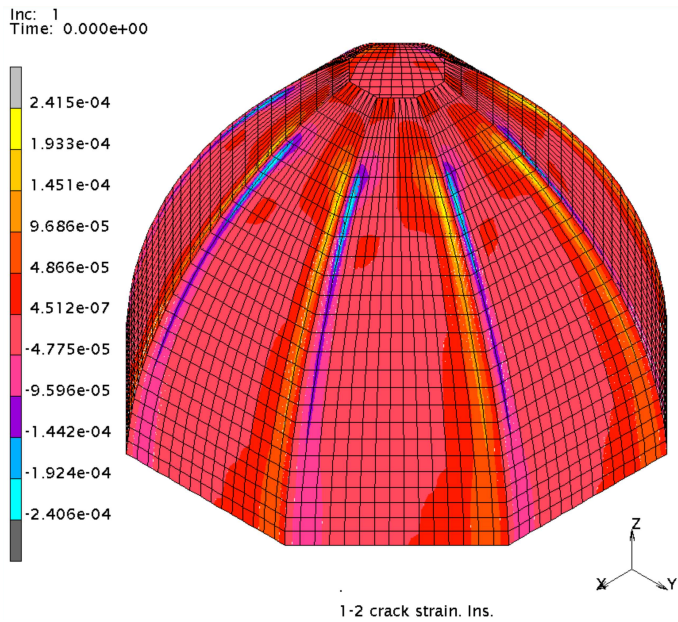


Figure 14. Component ε_{12}^f of the fracture strain in the intrados of the dome subjected to its own weight.

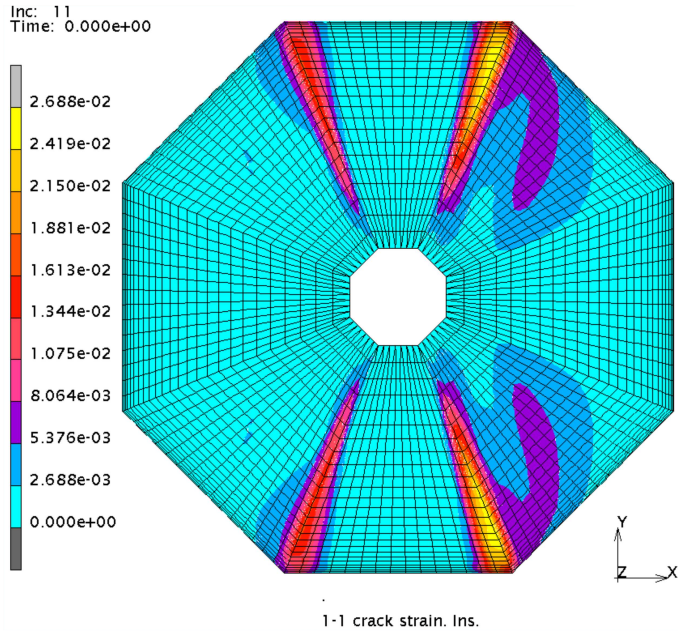


Figure 15. Component ε_{11}^f of the fracture strain at the intrados of the dome subjected to its own weight and a vertical displacement of the drum.

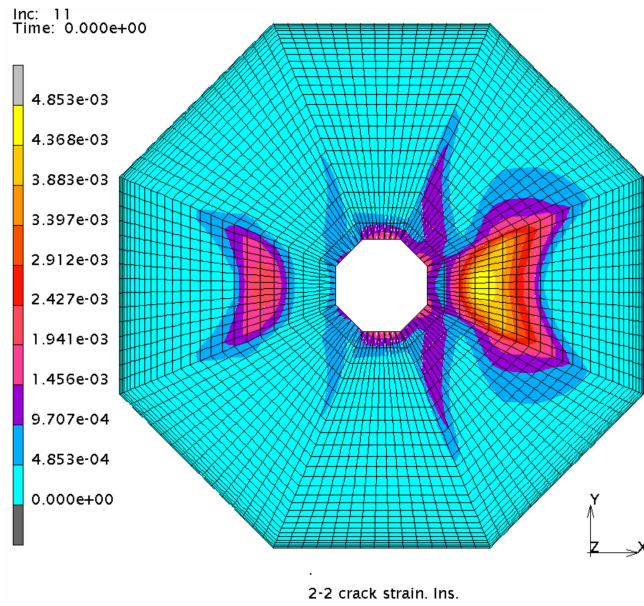


Figure 16. Component ε_{22}^f of the fracture strain at the intrados of the dome subjected to its own weight and a vertical displacement of the drum.

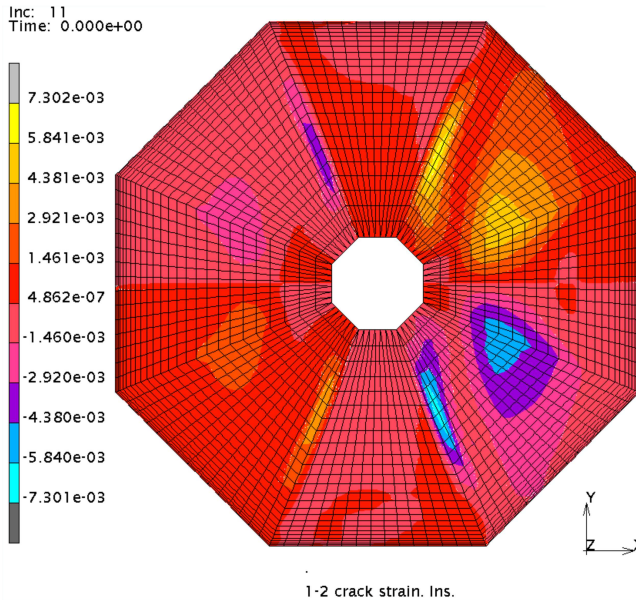


Figure 17. Component ε_{12}^f of the fracture strain at the intrados of the dome subjected to its own weight and a vertical displacement of the drum.

6. Conclusions

The methods proposed in this paper have proved to be useful in studying the static behavior of any kind of masonry vault subjected to very general load conditions, both for conducting collapse analyses and solving equilibrium problems. In particular, the study on the dome presented in Section 5.3 has shown that using suitable constitutive equations and appropriate numerical techniques to solve nonlinear problems enables determining the stress field, assessing vault safety on the basis of the derived maximum modulus eccentricity surface and, lastly, predicting the distribution and depth of eventual fracturing with good accuracy. Moreover, the ability to model variations in boundary conditions allows one to assess the behavior of a structure in the presence of settlement of the foundations, by determining the influence of such settlement on the stress field and the crack distribution.

References

- [Bennati and Padovani 1997] S. Bennati and C. Padovani, “Some non-linear elastic solutions for masonry solids”, *Mech. Struct. Mach.* **25**:2 (1997), 243–266.
- [Bernardeschi et al. 2004] K. Bernardeschi, C. Padovani, and G. Pasquinelli, “Numerical modelling of the structural behaviour of Buti’s bell tower”, *J. Cult. Herit.* **5**:4 (2004), 371–378.
- [Como 1992] M. Como, “Equilibrium and collapse analysis of masonry bodies”, *Meccanica (Milano)* **27**:3 (1992), 185–194.
- [Del Piero 1989] G. Del Piero, “Constitutive equation and compatibility of the external loads for linear elastic masonry-like materials”, *Meccanica (Milano)* **24**:3 (1989), 150–162.
- [Del Piero 1998] G. Del Piero, “Limit analysis and no-tension materials”, *Int. J. Plast.* **14**:1–3 (1998), 259–271.
- [Di Pasquale 1992] S. Di Pasquale, “New trends in the analysis of masonry structures”, *Meccanica (Milano)* **27**:3 (1992), 173–184.

- [Genna et al. 1998] F. Genna, M. Di Pasqua, M. Veroli, and P. Ronca, “Numerical analysis of old masonry buildings: a comparison among constitutive models”, *Eng. Struct.* **20**:1–2 (1998), 37–53.
- [Heyman 1966] J. Heyman, “The stone skeleton”, *Int. J. Solids Struct.* **2**:2 (1966), 249–256.
- [Heyman 1977] J. Heyman, *Equilibrium of shell structures*, Clarendon Press, Oxford, 1977.
- [Heyman 1982] J. Heyman, *The masonry arch*, Wiley, New York, 1982.
- [Livesley 1978] R. K. Livesley, “Limit analysis of structures formed from rigid blocks”, *Int. J. Numer. Methods Eng.* **12**:12 (1978), 1853–1871.
- [Livesley 1992a] R. K. Livesley, “The collapse analysis of masonry arch bridges”, pp. 261–274 in *Proceedings of the 4th Conference on Applied Solid Mechanics*, Elsevier, 1992.
- [Livesley 1992b] R. K. Livesley, “A computational model for the limit analysis of three-dimensional masonry structures”, *Meccanica (Milano)* **27**:3 (1992), 161–172.
- [Lourenço and Rots 1997] P. B. Lourenço and J. G. Rots, “Multisurface interface model for analysis of masonry structures”, *J. Eng. Mech. (ASCE)* **123**:7 (1997), 660–668.
- [Lourenço et al. 1998] P. B. Lourenço, J. G. Rots, and J. Blaauwendraad, “Continuum model for masonry: parameter estimation and validation”, *J. Struct. Eng. (ASCE)* **124**:6 (1998), 642–652.
- [Lucchesi and Zani 2003] M. Lucchesi and N. Zani, “Some explicit solutions to plane equilibrium problem for no-tension bodies”, *Struct. Eng. Mech.* **16**:3 (2003), 295–516.
- [Lucchesi et al. 1994] M. Lucchesi, C. Padovani, and A. Pagni, “A numerical method for solving equilibrium problems of masonry-like solids”, *Meccanica (Milano)* **29**:2 (1994), 175–193.
- [Lucchesi et al. 1996] M. Lucchesi, C. Padovani, and N. Zani, “Masonry-like solids with bounded compressive strength”, *Int. J. Solids Struct.* **33**:14 (1996), 1961–1994.
- [Lucchesi et al. 1999] M. Lucchesi, C. Padovani, G. Pasquinelli, and N. Zani, “The maximum modulus eccentricity surface for masonry vaults and limit analysis”, *Math. Mech. Solids* **4**:1 (1999), 71–87.
- [Lucchesi et al. 2000] M. Lucchesi, C. Padovani, A. Pagni, G. Pasquinelli, and N. Zani, “COMES-NOSA: A finite element code for non-linear structural analysis”, Technical report B4-2000-003, CNUCE, 2000.
- [Luciano and Sacco 1997] R. Luciano and E. Sacco, “Homogenization technique and damage model for old masonry material”, *Int. J. Solids Struct.* **34**:24 (1997), 3191–3208.
- [Maier et al. 1992] G. Maier, A. Nappi, and E. Papa, “Constitutive laws for engineering materials”, pp. 427–432 in *Damage models for masonry as a composite material: a numerical and experimental analysis*, edited by C. S. Desai, ASME Press, New York, 1992.
- [Nagtegaal and Slater 1981] J. C. Nagtegaal and I. G. Slater, “A simple nonconforming thin shell element based on discrete Kirchhoff theory”, pp. 167–192 in *Nonlinear finite element analysis of plates and shells*, edited by T. J. R. Hughes et al., AMD **48**, ASME, New York, 1981. Zbl 0511.00033
- [Orduña and Lourenço 2003] A. Orduña and P. B. Lourenço, “Cap model for limit analysis and strengthening of masonry structures”, *J. Struct. Eng. (ASCE)* **129**:10 (2003), 1367–1375.
- [Panzeca and Polizzotto 1988] T. Panzeca and C. Polizzotto, “Constitutive equations for no-tension materials”, *Meccanica (Milano)* **23**:2 (1988), 88–93.
- [Signorini 1925a] A. Signorini, “Un teorema di esistenza e unicità nello studio dei materiali poco resistenti a trazione”, *Rend. Accad. Naz. Lincei* **2** (1925), 401–406.
- [Signorini 1925b] A. Signorini, “Sulla pressoflessione delle murature”, *Rend. Accad. Naz. Lincei* **2** (1925), 484–489.
- [Theodossopoulos et al. 2002] D. Theodossopoulos, B. P. Sinha, A. S. Usmani, and A. S. J. Macdonald, “Assessment of the structural response of masonry cross vaults”, *Strain* **38**:3 (2002), 119–127.
- [Timoshenko and Woinowsky-Krieger 1987] S. P. Timoshenko and S. Woinowsky-Krieger, *Theory of plates and shells*, 2nd ed., McGraw-Hill, New York, 1987.
- [Trovalusci and Masiani 2005] P. Trovalusci and R. Masiani, “A multifield model for blocky materials based on multiscale description”, *Int. J. Solids Struct.* **42**:21–22 (2005), 5778–5794.

Received 8 May 2006. Accepted 18 Sep 2006.

MASSIMILIANO LUCCHESI: massimiliano.lucchesi@unifi.it

Dipartimento di Costruzioni, Università di Firenze, Piazza Brunelleschi 6, 50121 Firenze, Italia

CRISTINA PADOVANI: cristina.padovani@isti.cnr.it

Istituto di Scienza e Tecnologie dell'Informazione Alessandro Faedo, ISTI-CNR, Via G. Moruzzi 1, 56124 Pisa, Italia

GIUSEPPE PASQUINELLI: giuseppe.pasquinelli@isti.cnr.it

Istituto di Scienza e Tecnologie dell'Informazione Alessandro Faedo, ISTI-CNR, Via G. Moruzzi 1, 56124 Pisa, Italia

NICOLA ZANI: nicola.zani@unifi.it

Dipartimento di Costruzioni, Università di Firenze, Piazza Brunelleschi 6, 50121 Firenze, Italia